

Experimental analysis of biomimetic silencer to reduce exhaust noise in pneumatic devices

Min Hyeong Ahn^a, Jihoon Kim^a, Seung Ryeol Lee^b, Ui Deok Lee^c, Seunggi Kim^a, Dongjun Shin^b, Hyoungsoon Lee^{c,d,*}, Jaiyoung Ryu^{a,*}

^a School of Mechanical Engineering, Korea University Seoul, Seoul 02841, South Korea

^b Department of Mechanical Engineering, Yonsei University Seoul, Seoul 03722, South Korea

^c Department of Mechanical Engineering, Chung-Ang University Seoul, Seoul 06974, South Korea

^d Department of Intelligent Energy and Industry, Chung-Ang University Seoul, Seoul 06974, South Korea

ARTICLE INFO

Keywords:

Pneumatic device
Pneumatic artificial muscle
Noise reduction
Exhaust noise

ABSTRACT

Pneumatic devices such as pneumatic artificial muscles (PAMs) generate excessive noise during operation, thus inducing safety hazards and becoming a nuisance to nearby communities. In this study, biomimetic silencers consisting of polyurethane foam and slit structures that mimic shark gill slits to reduce the exhaust noise caused by pneumatic devices were developed and experimentally analyzed. Two separate experimental approaches were employed to evaluate and analyze the performance of the developed biomimetic silencer. During these experiments involving the compressor and PAM exhaust noise measurements, the sound pressure signals, noise, and flow rate were obtained for the cases of with and without silencer. The results demonstrated that the slit structure of the developed silencer decreased the relative velocity with the surrounding air, thus resulting in approximately 6 dB improvement in noise reduction performance of the developed silencer compared with that of a general pneumatic silencer. Although the use of porous materials in the silencer causes an exhaust time delay, the delay is insignificant compared with that of a general pneumatic silencer in terms of the exhaust area. Thus, the developed silencer is an effective solution for reducing the exhaust noise in pneumatic devices, particularly in situations where noise reduction is critical.

1. Introduction

Pneumatic devices, such as pneumatic artificial muscles (PAMs), have garnered significant attention in recent decades owing to their efficiency, reliability, and cost-effectiveness. However, the exhaust of compressed air during operation generates aerodynamic noise, which causes safety hazards and becomes a nuisance for workers and nearby communities. Compared with other pneumatic devices used in various industrial fields, PAMs employ high-pressure compressed air to operate devices such as wearable robots [1–5]. The aerodynamic noise generated during the process of exhausting the compressed air into the atmosphere is a significant concern, as pneumatic devices are commonly employed in many industrial fields. In particular, PAMs are frequently employed in mobile or wearable robots for daily use. Exposure to loud or continuous noise can lead to annoyance, stress, sleep disturbances, and diseases associated with these conditions [6,7].

Numerous studies have developed and analyzed noise reduction

devices and methods for pneumatic devices in various fields [8–11]. Li and Zhao [12,13] investigated the acoustic properties of a silencer that utilized sintered bronze to reduce the exhaust noise of a pneumatic friction clutch and brake (PFC/B) system. They analyzed the characteristics of the impulse exhaust noise generated during the sudden exhaust of the PFC/B system through the valve opening process and studied the relationship between the exhaust time delay and noise reduction. Laffay et al. [14] conducted an experimental study on the noise reduction and characteristics of high-pressure exhaust flow through diaphragms and perforated plates. Although several studies have attempted to reduce the exhaust noise of pneumatic devices, few have focused on reducing the exhaust noise of PAMs. In a study on devices using PAM, Duran [1] used a general pneumatic silencer with porous materials to reduce the exhaust noise of the PAM. The study indicated that the use of a silencer decreases the exhaust airflow and may interfere with the operation of the PAM. Moreover, current pneumatic silencers use porous materials, such as polymers or bronze, which

* Corresponding authors.

E-mail addresses: leeh@cau.ac.kr (H. Lee), jryu@korea.ac.kr (J. Ryu).

<https://doi.org/10.1016/j.apacoust.2023.109681>

Received 26 April 2023; Received in revised form 16 August 2023; Accepted 1 October 2023

Available online 8 October 2023

0003-682X/© 2023 Elsevier Ltd. All rights reserved.

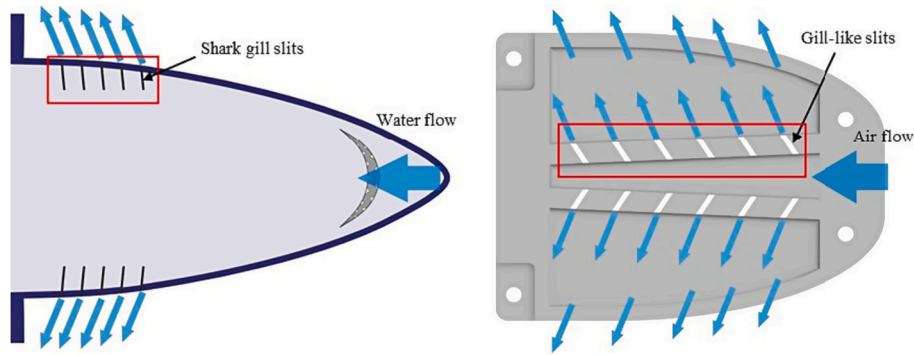


Fig. 1. Biomimetic design of pneumatic silencer inspired by shark gill slits.

cause little delay in the exhaust time; however, the noise reduction effect is insufficient.

Porous materials, such as sintered polymers, are effective in reducing noise levels in general pneumatic silencers. Polyurethane foams are also commonly used as a readily available sound-absorbing material [15]. The soft polyurethane foam implemented within the developed silencer exhibited outstanding performance in reducing the noise level, particularly at medium and high frequencies [16]. Therefore, incorporating polyurethane foam into the shark gill structure could potentially further enhance its noise reduction performance.

Many researchers have utilized the characteristics of nature as a source of inspiration to solve problems. Biomimetics is the method of designing or advancing science and technology by mimicking the characteristics of nature. Several studies investigated the use of biomimicry. For instance, Ye et al. [17] explored the use of a shark fin structure to reduce the noise generated by the wake of a car's side mirror, whereas Kim et al. [18] investigated the implementation of a shark gill slit structure to reduce the maximum pressure gradient of the compression wave at the entrance of a tunnel. Moreover, Ibrahim et al. [19] investigated the reduction in vibration of rod bundle caused by jet flow by biomimicking a shark-gill-like slit structures.

A biomimetic silencer has been designed based on the breathing technique of sharks. Fig. 1 shows a schematic of the respiration process in sharks and the development of a pneumatic silencer based on this principle. Sharks use a method called “ram ventilation” to breathe [20], in which they open their mouth to absorb and release oxygen through their gills. From an engineering perspective, the water ejected through the gill slits forms a jet in the cross flow. Ibrahim et al. [19] observed that the design of gill slits enhanced the mixing between the jet flow and the surrounding fluids, thus leading to a reduction in the relative velocity of the jet and the surrounding water, which results in faster jet velocity reduction. In addition, the design of the shark-gill-like slit structures can help minimize the pressure drop across the silencer. Therefore, a biomimetic design approach was utilized to further reduce the noise level without significantly delaying the exhaust time, and the

shape of the silencer was inspired by the structure of the shark gill slits.

Compressed air from the nozzles of pneumatic devices, such as PAM, resembles jets coming out through shark gill slits and exhibits the characteristics of a jet. The jet noise generated by this method has been extensively studied experimentally and theoretically over the past decades, as it is an important noise source not only in aircraft but also in pneumatic devices such as the PAM. According to Lighthill's [21–23] study on jet noise, the most effective way to reduce jet noise is to reduce the jet speed. Another way to reduce jet noise radiation is to decrease the RMS turbulent velocity by reducing the relative velocity of the jet and the surrounding air. Therefore, to reduce the jet noise generated by the exhaust of the PAM, a silencer that mimics the gill slit structure of a shark and applies the noise reduction principle was developed.

The study aimed to experimentally analyze the developed silencer to reduce the exhaust noise caused by the operation of a pneumatic system, such as a PAM. Therefore, this study involved two experimental analyses to evaluate the SPL reduction of exhaust noise of pneumatic devices. First, the sound pressure signals, noise, and flow rate of the compressed air exhausted from the compressor were measured. The noise reduction performance of the shark gill-like slits silencer developed for general pneumatic systems was evaluated and compared with that of a general pneumatic silencer. Subsequently, the sound pressure signals, noise, and flow rate of the compressed air exhausted during the operation of the PAM were measured. Based on the experimental results, the effect of the silencers on the operation of the PAM and the level of noise reduction were analyzed. A higher level of noise reduction is required to ensure that the PAM operates smoothly with little delay in the exhaust time and without causing noise-related problems in daily life. In this study, a silencer with a high level of noise reduction was developed and evaluated by applying a porous material along with a structure that mimicked shark gill slits.

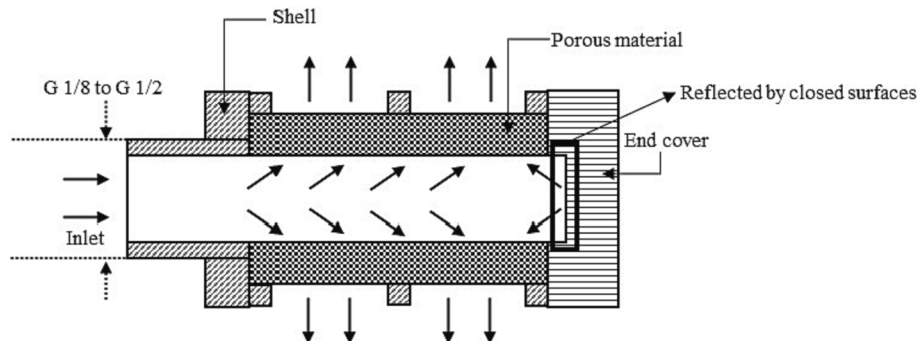


Fig. 2. Structure of general pneumatic silencer.

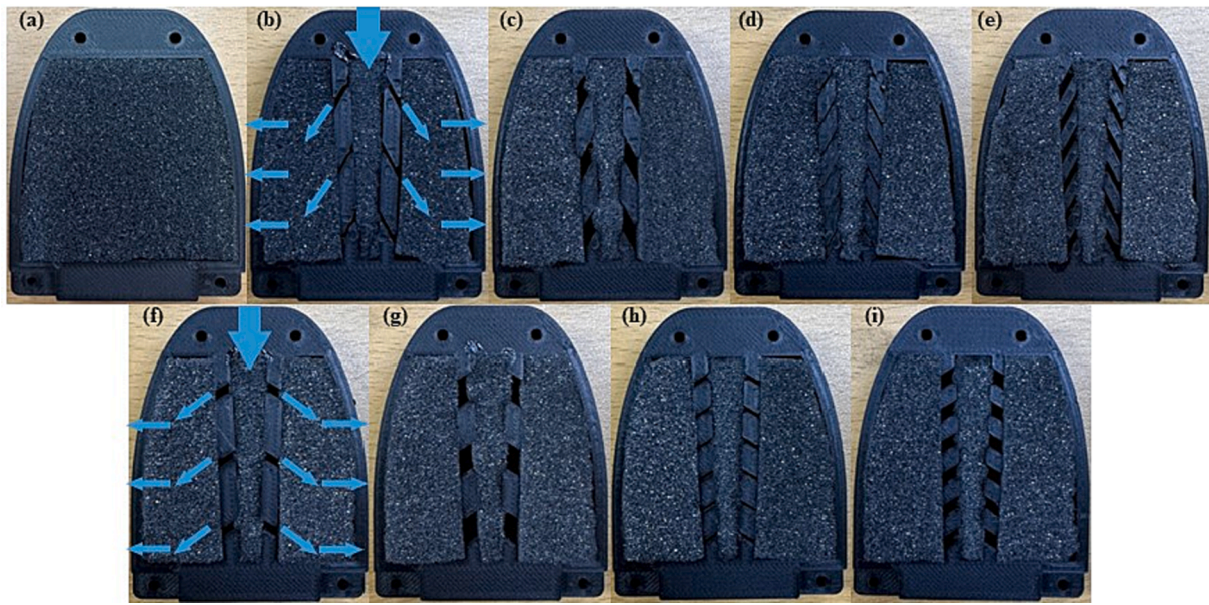


Fig. 3. Pneumatic silencers developed with biomimetic shark gill slits: (a) NS, (b) 3D3S2M, (c) 3D3S6M, (d) 3D6S1M, (e) 3D6S3M, (f) 6D3S2M, (g) 6D3S6M, (h) 6D6S1M, and (i) 6D6S3M. (Blue arrows represent flow direction inside the silencer.).

Table 1
Geometric characteristics of the developed pneumatic silencer slits.

Case	A (°)	N	S (cm ²)	D (cm)
NS	–	–	–	–
3D3S2M	30	6	1.08	0.2
3D3S6M	30	6	3.24	0.6
3D6S1M	30	12	1.08	0.1
3D6S3M	30	12	3.24	0.3
6D3S2M	60	6	1.08	0.2
6D3S6M	60	6	3.24	0.6
6D6S1M	60	12	1.08	0.1
6D6S3M	60	12	3.24	0.3

2. Method

2.1. Silencer specification

A general cylindrical pneumatic silencer comprising a silencer shell, porous material, and an end cover, with structure and dimensions as illustrated in Fig. 2, was used in the experiment. General pneumatic silencers have four different sizes—G 1/8, G 1/4, G 3/8, and G 1/2—according to the size of the ISO 228-1 standard parallel threads used as fitting tools for connecting the silencer and the pneumatic device. The four different cases were named G1, G2, G3, and G4 according to their respective sizes, and the general pneumatic silencers used sintered polyurethane as the porous material. In contrast to general pneumatic silencers, this new design is intended to mimic shark-gill-like slit structures. Fig. 3 shows the nine silencers tested in this study, all of which have the same size of 5 cm × 6.5 cm × 1.3 cm (width × length × height).

To investigate the noise reduction effect of the silencer containing slits that mimic shark gill slits, two models were produced: one without slits and one with slits. Table 1 presents the geometric characteristics of the slits, including the angle (A), number of slits (N), total area (S), and spacing of the slits (D). The performance of the silencer was compared based on each parameter, and the number of slits (N) and spacing of the slits (D) were varied in relation to the total area (S) of the slits. The noise reduction effects of the slits were evaluated for eight cases with varying numbers of slits and the results were compared with those of the case of no slits (NS). The angles of the slits were set at 30° and 60° based on the

Table 2
Summary of exhaust area for general pneumatic silencers and the developed silencers.

Case	Exhaust area (cm ²)
G1	5.873
G2	12.979
G3	25.571
G4	43.545
Developed silencers	5.14

centerline of the inlet of the silencer, and the cases included those with large and small slit areas for each angle. We conducted experiments on nine silencer cases that mimic shark gill slits, including the NS case, to evaluate their performance in terms of noise reduction and exhaust time delays. Additionally, the exhaust areas of the general pneumatic silencer and the developed silencer are summarized in Table 2; the exhaust area of the developed silencer is similar to that of the smallest case, G1, of the general pneumatic silencer.

The scanning electron microscopy (SEM) images of the sintered polyurethane and polyurethane foam used in the silencers are presented in Fig. 4 [24]. The porosity of the two types of polyurethane used in each silencer was determined through image processing using ImageJ software. Porosity refers to the percentage of the image area that corresponds to empty spaces or pores within the material and is calculated by dividing the pore area by the total area of the image and multiplying the result by 100. Fig. 4(a) shows the SEM image of sintered polyurethane foam commonly used in general pneumatic silencers, which has a porosity of 17.3, whereas Fig. 4(b) shows the polyurethane foam used in the developed silencer, which has a higher porosity of 30.6.

2.2. Experimental method

2.2.1. Experimental setup

The experiments were performed in an experimental room at Chung-Ang University to minimize background noise. The size of the experimental room was 4.4 m × 4.0 m × 3.0 m and the background noise was set below 30 dB of the overall sound pressure level (OASPL). First, the experimental equipment was configured as shown in Fig. 5(a) to determine the effect of each silencer in a large frame when air was

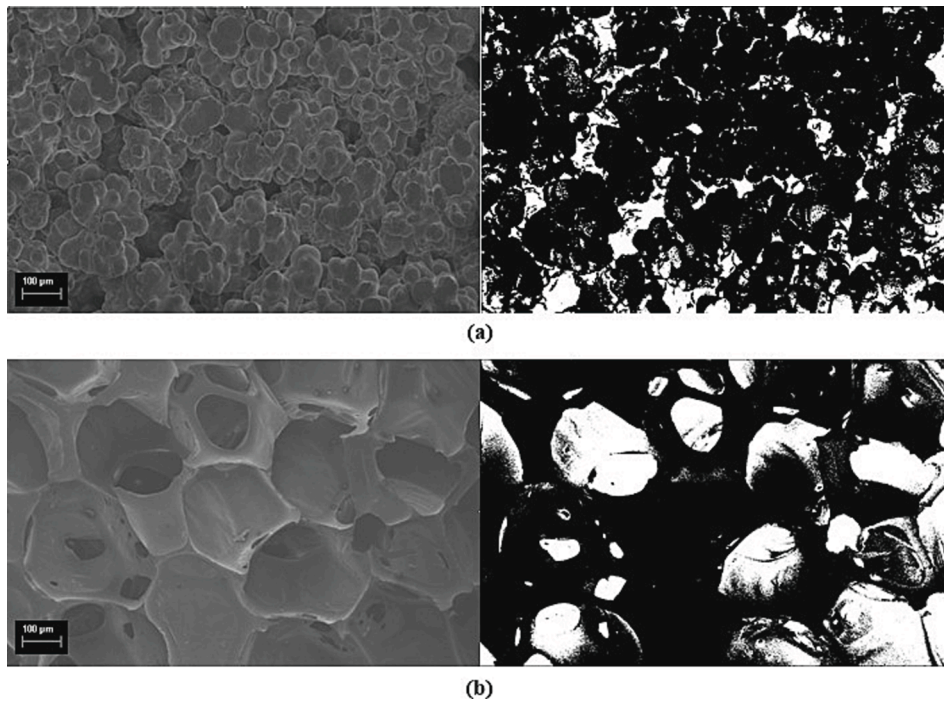


Fig. 4. SEM images and image processing results: (a) General pneumatic silencer and (b) developed pneumatic silencer.

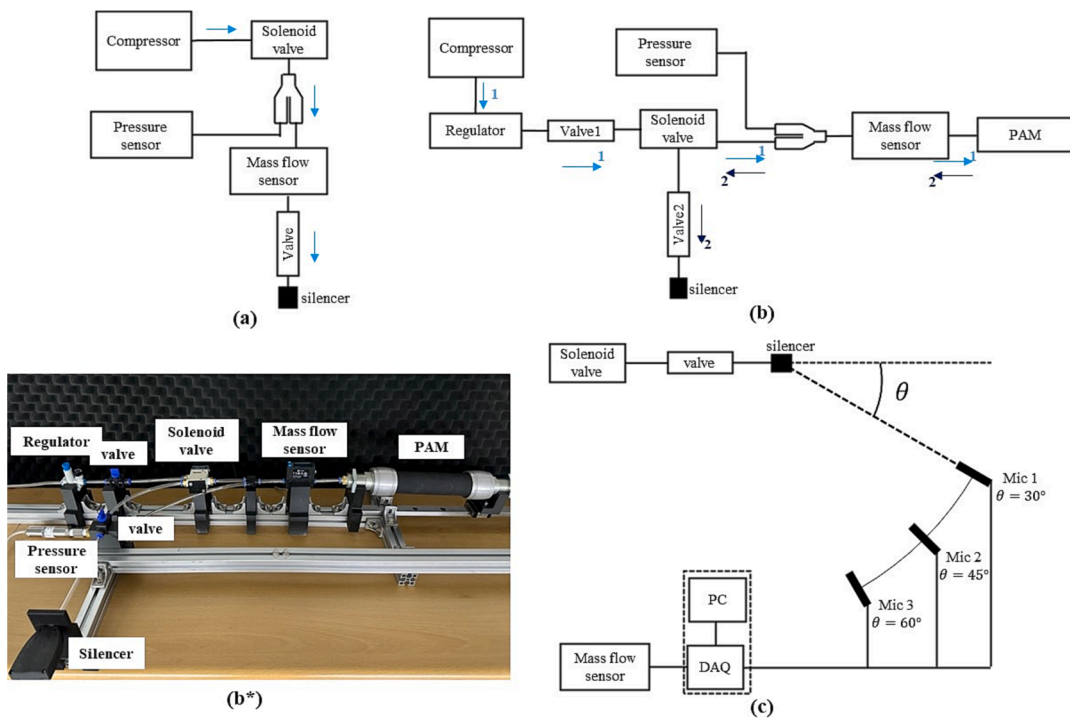


Fig. 5. Experimental setup for measuring compressor and PAM exhaust noise. (a) Compressor exhaust noise measurement setup, (b) PAM exhaust noise measurement setup, (b*) photograph of experimental equipment, and (c) schematic of microphone array positions.

directly exhausted through the compressor. This experiment demonstrated that a silencer that mimics shark gill slits could reduce noise in general pneumatic devices. As shown in Fig. 5(a), the experimental setup consisted of a compressor, solenoid valve, and apparatus to measure flow characteristics, including pressure and FESTO SFAH-200U-Q6S-PNLK-PNVRA-L1 mass flow sensors. For the subsequent experiment, the configuration of the experimental equipment was set by referring to the pneumatic system with a single 3-way valve used by

Xavier et al. [25], as shown in Fig. 5(b). The experimental equipment consisted of a compressor, pressure regulator, PAM, 3-way solenoid valve, and pressure and mass flow sensors. A photograph of the experimental equipment is presented in Fig. 5(b*). In all experiments, the equipment was connected to a tube with an outer diameter of 6 mm and inner diameter of 4 mm.

Acoustic measurements were performed using microphone arrays with a radius of 1 m and the outlet of the pneumatic system as the center

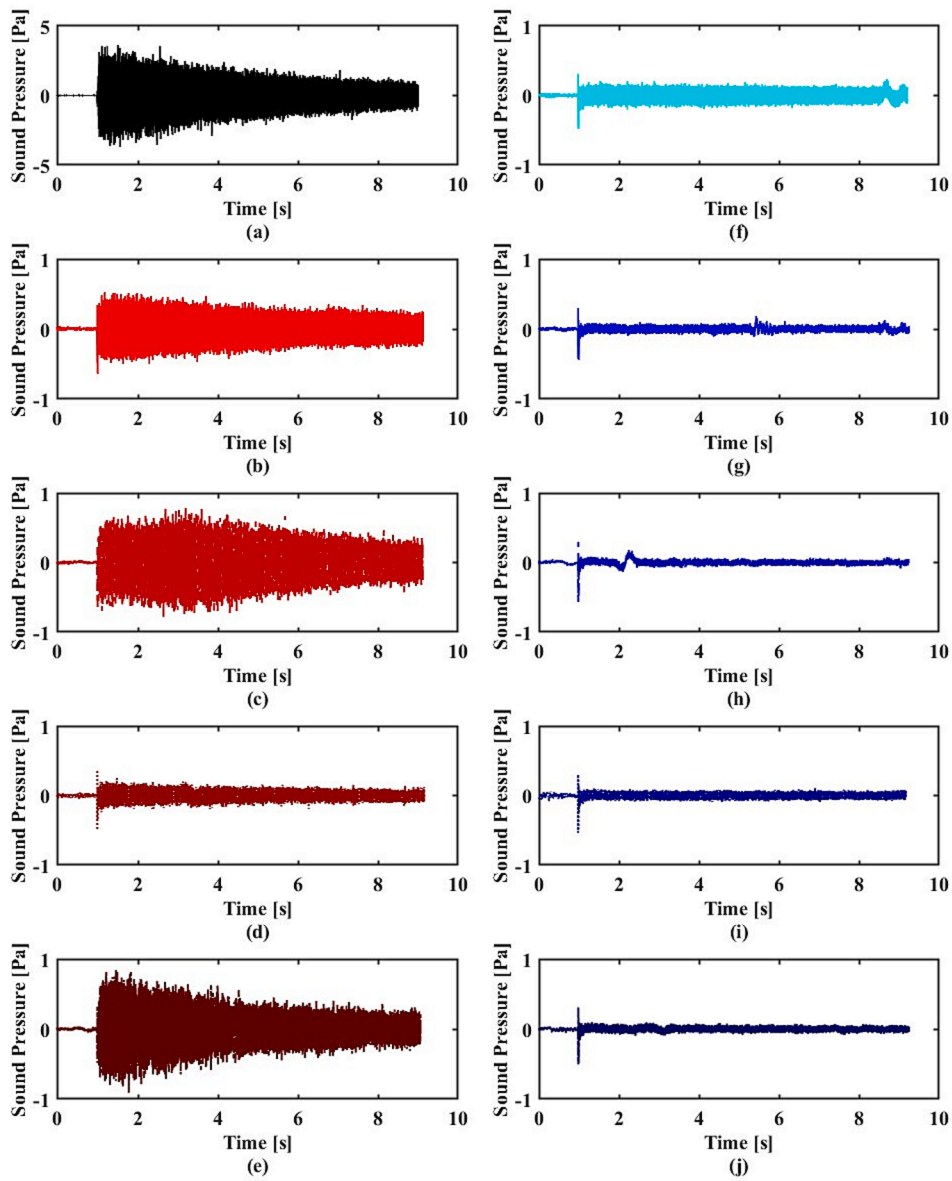


Fig. 6. Sound pressure of the compressor exhaust noise measured at $\theta = 45^\circ$: (a) Reference, (b) G1, (c) G2, (d) G3, (e) G4, (f) NS, (g) 6D3S2M, (h) 6D3S6M, (i) 6D6S1M, and (j) 6D6S3M.

[26]. As it was necessary to measure the influence of jet noise directivity of all cases, we employed a configuration of three microphone arrays. The microphone array used three PCB 130f20 microphones and was configured as shown in Fig. 5(c) from $\theta = 30^\circ$ to $\theta = 60^\circ$ at intervals of 15° , where θ is defined as the angle between the center axis and the exhaust outlet of the pneumatic systems. The microphone has a diameter of 1/4 in and sensitivity of 45 mV/Pa. To prevent interference with the high-frequency acoustic measurements of the microphone, the protective grid cap was removed. Acoustic signal measurement data and flow measurement data were continuously recorded in real time using the National Instruments sound and vibration input module NI-9234. The measurement data were transmitted to a computer using a National Instruments cDAQ-9171.

2.2.2. Test procedure

Two test procedures were performed to evaluate the performance of the shark gill-simulated silencer in a typical pneumatic system. The first procedure involved the use of a compressor and solenoid valve to measure the noise reduction performance. When the compressor

pressure reached 8 bar, the experiment was conducted until the flow rate at the outlet reached a certain level during the exhaust process. Pressure and flow sensors were installed between the 3-way solenoid valve and outlet to measure the exhaust pressure from the air compressor.

The second procedure involved connecting the PAM to an air compressor through a pressure regulator and solenoid valves. The compressor filled the PAM with air through a solenoid valve, whereas the regulator maintained a constant pressure inside the PAM by adjusting the pressure from the compressor.

The PAM pressure was set to 4, 6, and 8 bar using the regulator. After filling the air inside the PAM, the direction of the valve was changed to exhaust the air into the atmosphere. Pressure and flow sensors were installed between the 3-way solenoid valve and the PAM to measure the exhaust pressure from the PAM.

To evaluate the noise reduction performance of the silencers, they were connected to the exhaust outlet of the pneumatic system. Real-time sound pressure measurements were obtained using microphone arrays when the compressed air was exhausted from either the compressor or the PAM. These experimental cases allowed the evaluation of the

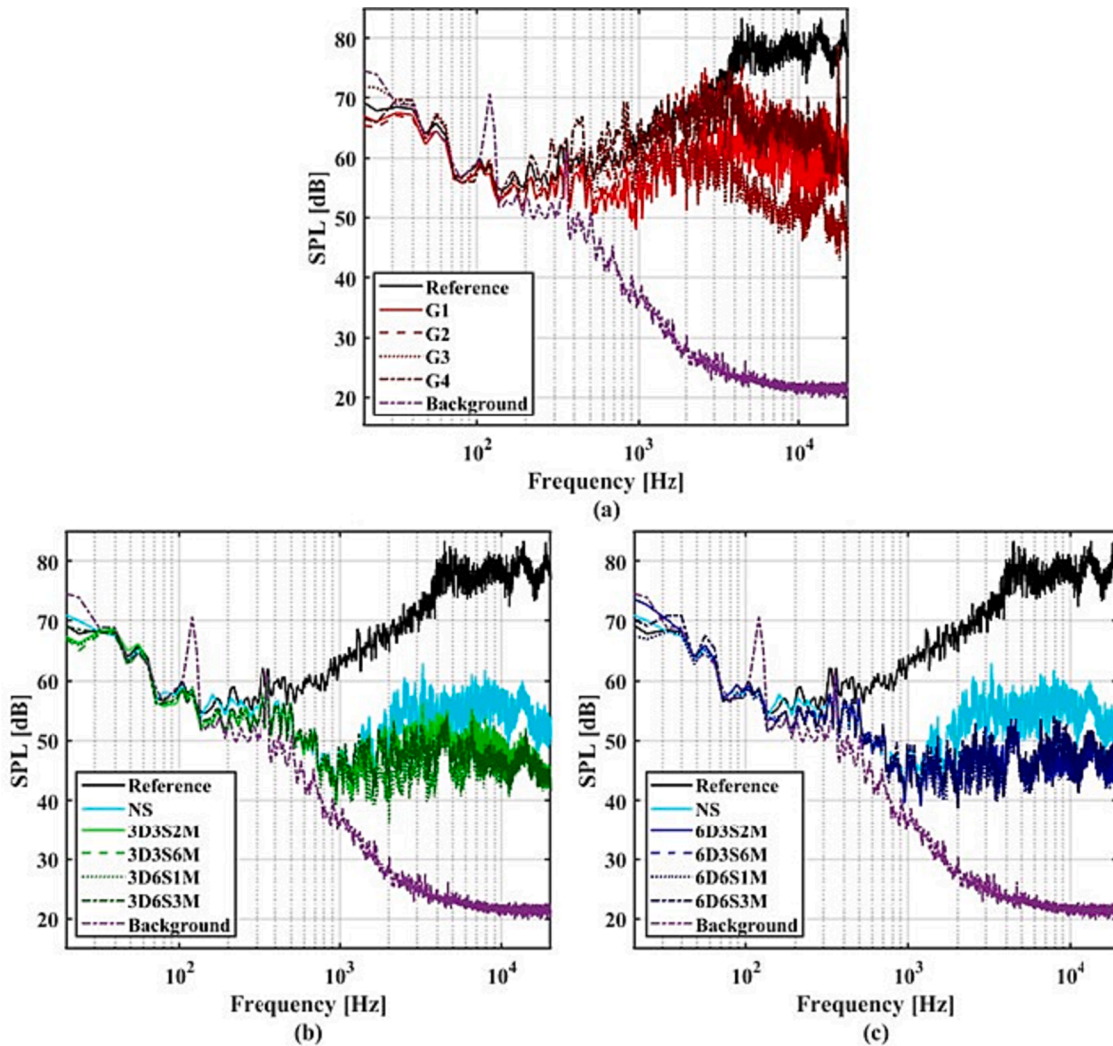


Fig. 7. SPL spectra of pneumatic silencers at microphone angle of $\theta = 45^\circ$: (a) general pneumatic silencer, (b) developed pneumatic silencer with 30° slit angle, and (c) developed pneumatic silencer with 60° slit angle.

silencer performance in terms of noise reduction and delay in exhaust time.

3. Experimental results and discussions

Acoustic measurements were conducted to compare the noise reduction performances of general pneumatic silencers and silencers that mimic shark gill slits. The power spectral density (PSD) of the sound pressure was obtained using the Pwelch function of Welch's PSD estimate method in MATLAB based on the sound pressure data. The Pwelch function used a frequency resolution of $df = 8$ Hz and applied a Hanning window with 50% overlap. Parseval's theorem equation was used to calculate the sound pressure level (SPL), as follows [27]:

$$\sum_{f=0}^{L-1} PSD(f)df = 1/L \left(\sum_{l=0}^{L-1} |x(l)^2| \right), \quad (1)$$

where $PSD(f)$ is the PSD estimated using the Pwelch method, df is the frequency resolution, and L is the number of samples in the time-domain signal $x(l)$. Using this theorem, the SPL can be calculated as follows:

$$SPL(f) = 10 \log \left(\left(PSD(f) \sqrt{Ldf} \right) / (p_{ref}^2) \right), \quad (2)$$

where $p_{ref} = 2 \times 10^{-5} (Pa)$ is the reference SPL for air. To obtain the

OASPL value of each silencer, the signal between 100 and 20,000 Hz was processed using the following equation, considering the human audible frequency range.

$$OASPL = 10 \log \left(\left(\sum_{100}^{20,000} PSD(f) \sqrt{Ldf} \right) / p_{ref}^2 \right) \quad (3)$$

3.1. Acoustic measurement of compressor exhaust flow

This study attempted to measure and analyze the effects of different silencer cases on the compressor exhaust noise under the operating conditions of a general pneumatic system. As mentioned in Section 2.2.2, the air in the compressor was filled to 8 bars, and the exhaust was opened while measuring the sound level; subsequently, when the total flow measured by the flow sensor reached a certain value, the solenoid valve was closed. The sound pressure data in the time domain from 1 s were measured for the exhaust noise with the solenoid valve opening.

Fig. 6 shows the sound pressure fluctuation graph measured at $\theta = 45^\circ$. In several cases, a noise peak occurred at 1.1 s, thus indicating that the noise generated by the large flow was exhausted simultaneously owing to the operation of the solenoid valve. A rapid decrease in the sound pressure was observed in cases G3 and 6D. Compared with the reference case, the sound pressure ranges of the cases with silencers were significantly reduced; therefore, the sound pressure ranges of the

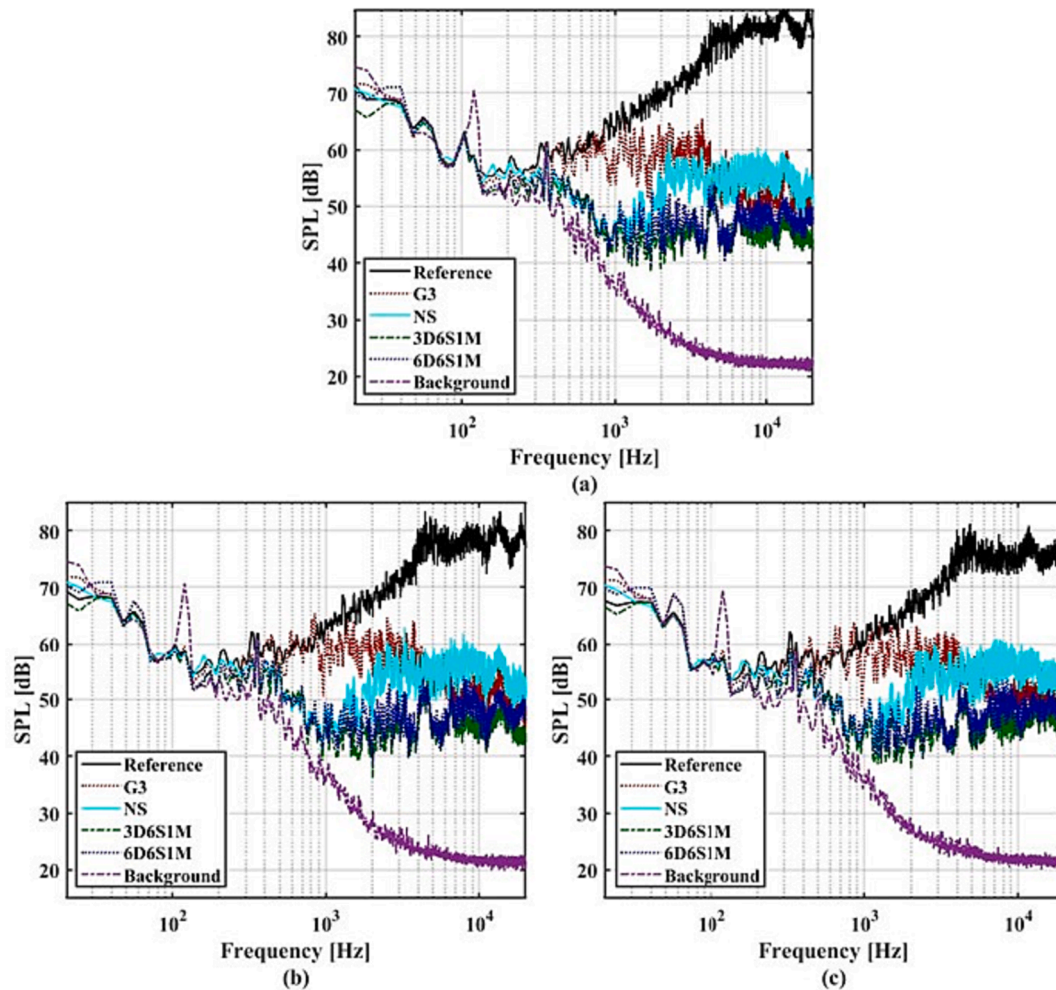


Fig. 8. Comparison of SPL spectra of pneumatic silencers: (a) $\theta = 30^\circ$, (b) $\theta = 45^\circ$, and (c) $\theta = 60^\circ$.

cases excluding the reference case were adjusted. The cases with general pneumatic silencers, including G1, G2, and G4 in Fig. 6(a), exhibited an increase in the sound pressure shortly after the exhaust release began, followed by a linear decrease in the fluctuation width. Fig. 6(d) shows a sound pressure fluctuation pattern similar to those of the NS and 6D cases. Noise was generated by the solenoid valve exhaust and a significant decrease in the sound pressure fluctuation was observed.

In Fig. 7, the SPL spectra, which assess the noise based on frequency as an evaluation metric for noise reduction, obtained using the Pwelch method are shown for the general pneumatic silencer, 3D cases, and 6D cases. At $\theta = 45^\circ$, the sound pressure data measured through a microphone were used. In the reference case, the SPL gradually increased at the middle frequency, and the peak frequencies appeared at approximately 4, 13, and 18 kHz. Fig. 7(a) shows a comparison of the SPL for G silencers of different sizes. In the cases G1, G2, and G4, the SPL was high at the middle frequency, and the peak frequencies matched those observed in the reference case. An additional peak frequency was observed at approximately 17 kHz in G2 and G4. The G3 case exhibited the lowest SPL among the general pneumatic silencers, with a decrease in the SPL of more than approximately 4 kHz. Fig. 7(b) and (c) present the SPL results for cases with different slit distances and numbers for slit angles of 30° and 60° . Unlike general pneumatic silencers, they exhibited a tendency for the SPL to decrease at the middle frequency and decrease more sharply at high frequencies. Moreover, the peak frequencies matched those in the reference case. The NS case showed a relatively high SPL compared with the cases with slits, and it did not show peak frequencies at the middle frequency, as in the previous cases.

In the 3D cases, the SPL of 3D6S1M and 3D6S3M were lower than those of the other cases.

To compare the SPLs of each silencer, Fig. 8 displays the 6S1M cases with slit angles of 30° and 60° and the G3 case of the general pneumatic silencer. Fig. 8 shows the SPL spectrum displaying the SPL values at microphone angles of $\theta = 30^\circ$, 45° , and 60° . In the reference case, the SPL at high frequencies decreased as the angle increased. The shark-gill-like slits silencer cases showed a lower SPL at the middle frequency compared with the general pneumatic silencer.

When comparing the G3 and NS cases at high frequencies, the G3 case exhibited a lower SPL. In addition, when slits were added to the shark-gill-like slits silencer cases, they showed a decrease in the SPL at high frequencies compared with the NS case without slits, and the decrease in the SPL was greater than that in the G3 case. With increase in the microphone angle, the SPL exhibited a decreasing trend in both the reference and G3 cases. However, in the developed silencer, the variation in the SPL with respect to angle was insignificant.

To investigate the overall magnitude of noise according to the angle, A-weighted octave bands (L_A) were applied to the SPL spectrum graphs shown in Figs. 9 and 10 to determine the OASPL and L_A according to the frequency. The OASPL, which assess the overall noise reduction in the frequency range, was calculated using Eq. (3). The results indicated that the general pneumatic silencer case, which was the most effective in the previous analysis, corresponded to the G3 case; all shark-gill-like slits silencer cases were additionally plotted.

The OASPL values shown in Fig. 9 are listed in Table 3. First, for G3, the OASPL value decreased as the angle increased. At $\theta = 30^\circ$, the

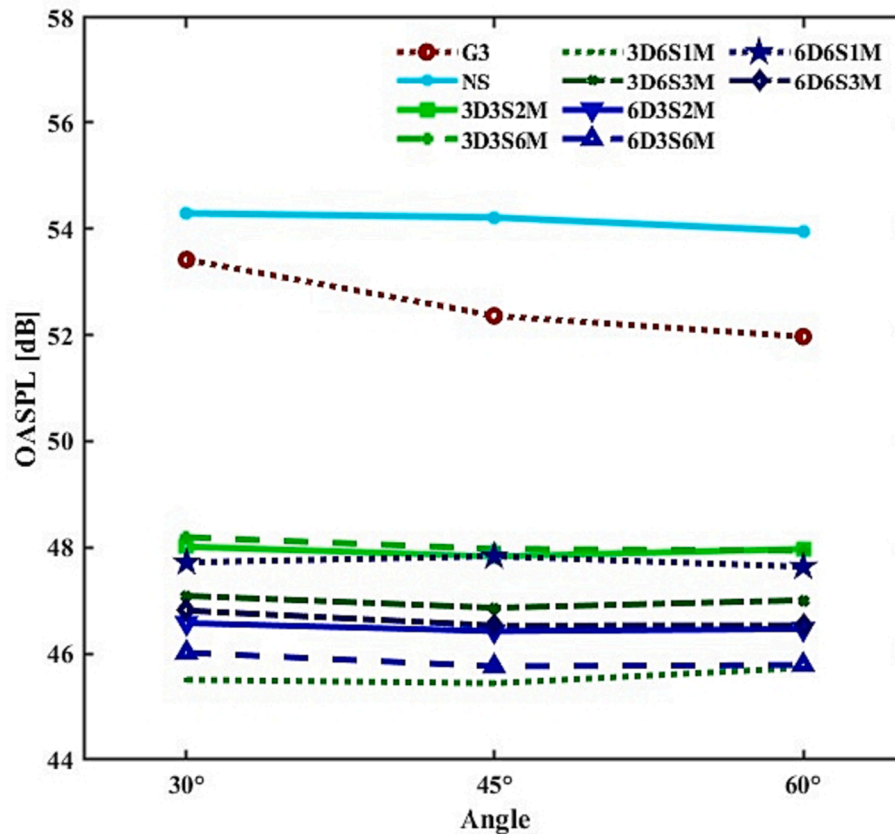


Fig. 9. Comparison of OASPL between general and developed pneumatic silencers at $\theta = 30^\circ$, 45° , and 60° .

OASPL was approximately 54.3 dB for NS, whereas it was approximately 53.4 dB for G3, thus indicating a decrease in OASPL of approximately 1 dB. However, at 60° , the OASPL was 53.9 dB for NS whereas 51.9 dB for G3, thus indicating a decrease of 2 dB. In addition, when comparing the noise reduction effects, in the G3 case, the OASPL decreased by 7.4 and 7.9 dB, respectively, at $\theta = 30^\circ$, and by 6.2 and 6.3 dB, respectively, at $\theta = 60^\circ$. When comparing the OASPL of the reference and silencer cases, at $\theta = 30^\circ$, the OASPLs of the G3, 3D6S1M, and 6D3S6M cases decreased by 25.7, 33.6, and 33.1 dB, respectively. The OASPLs of 3D6S1M and 6D3S6M were all below 46 dB at all angles.

The noise reduction effects of the most effective cases, namely 3D6S1M and 6D3S6M, were analyzed using the A-weighted octave band SPL spectrum, which assess the SPL perceived by the human ear across each frequency band, based on Fig. 9 and Table 3. The results are shown in Fig. 10. In the reference case, L_A at high frequencies was higher at 30° microphone measurement angle than at 45° and 60° , with a peak L_A of 80.05 dBA at 4 kHz (b). In addition, L_A of G3 was higher than that of NS up to 4 kHz; however, NS exhibited a higher L_A above 8 kHz. Notably, for the 3D6S1M and 6D3S6M cases, L_A decreased significantly above 2 kHz frequency compared with the NS model without slits.

In summary, based on the SPL and OASPL results, the exhaust noise from the compressor decreased by approximately 28 dB at $\theta = 60^\circ$ in the 3D6S1M and 6D3S6M cases compared with the reference case, and decreased by more than 6 dB compared with the exhaust noise of general pneumatic silencers.

3.2. Exhaust time delay and delay rate analysis of pneumatic silencers

During the operation of pneumatic devices, compressed air is discharged into the atmosphere, and the exhaust time is related to the device performance. In pneumatic devices, such as PAM, the actuation

for contraction and other movements is instigated by the release of compressed air. Therefore, if a delay exists in the exhaust timeframe, it leads to an increase in the contraction time, which inevitably results in diminished performance. Therefore, the exhaust delay caused by the silencer must be determined. To accomplish this, we measured the time difference between when the exhaust air volume (V , the cumulative value of the flow rate measured by a flow sensor over time) reached a certain level and when the exhaust stopped, in the event of the compressed air being exhausted from the compressor. The exhaust air volume over time is shown in Fig. 11. In the reference case without a silencer, measurements were taken from 1 s of exhaust to 9 s when the exhaust air volume reached 0.024 m^3 . For each case with a silencer, measurements were taken until the exhaust air volume reached the level measured in the reference case. The delay rate (DR), calculated as the ratio of the time delay to that in the reference case, is presented in Table 4 and indicates the time delay due to the silencer. The following equation was used to calculate the DR.

$$DR = (t_s - t_r) / (t_r - t_i) \times 100\% \quad (4)$$

t_s represents the time when the silencer case reached the reference exhaust air volume, and t_r represents the time when the reference case reached the reference exhaust air volume, which was 9 s; $t_s - t_r$ represents time delay of exhaust caused by silencer; and t_i represents the start time of the exhaust, with a value of 1 s. Among the general pneumatic silencers, G3 exhibited the best noise reduction performance, with an exhaust time delay of approximately 0.16 s and DR of approximately 2.0%. Among the developed silencers, the 3D case exhibited the greatest exhaust time delay in the 3D3S2M case, whereas the 3D6S1M case, which had the best noise reduction effect, exhibited an exhaust time delay of 0.35 s, resulting in a DR of 4.3%. Among the 3D cases, the DR of 3D6S3M was the highest at 3.3%. The 6D3S6M case had an exhaust time delay of 0.25 s and DR of 3.1%. Furthermore, the 6D6S1M case showed

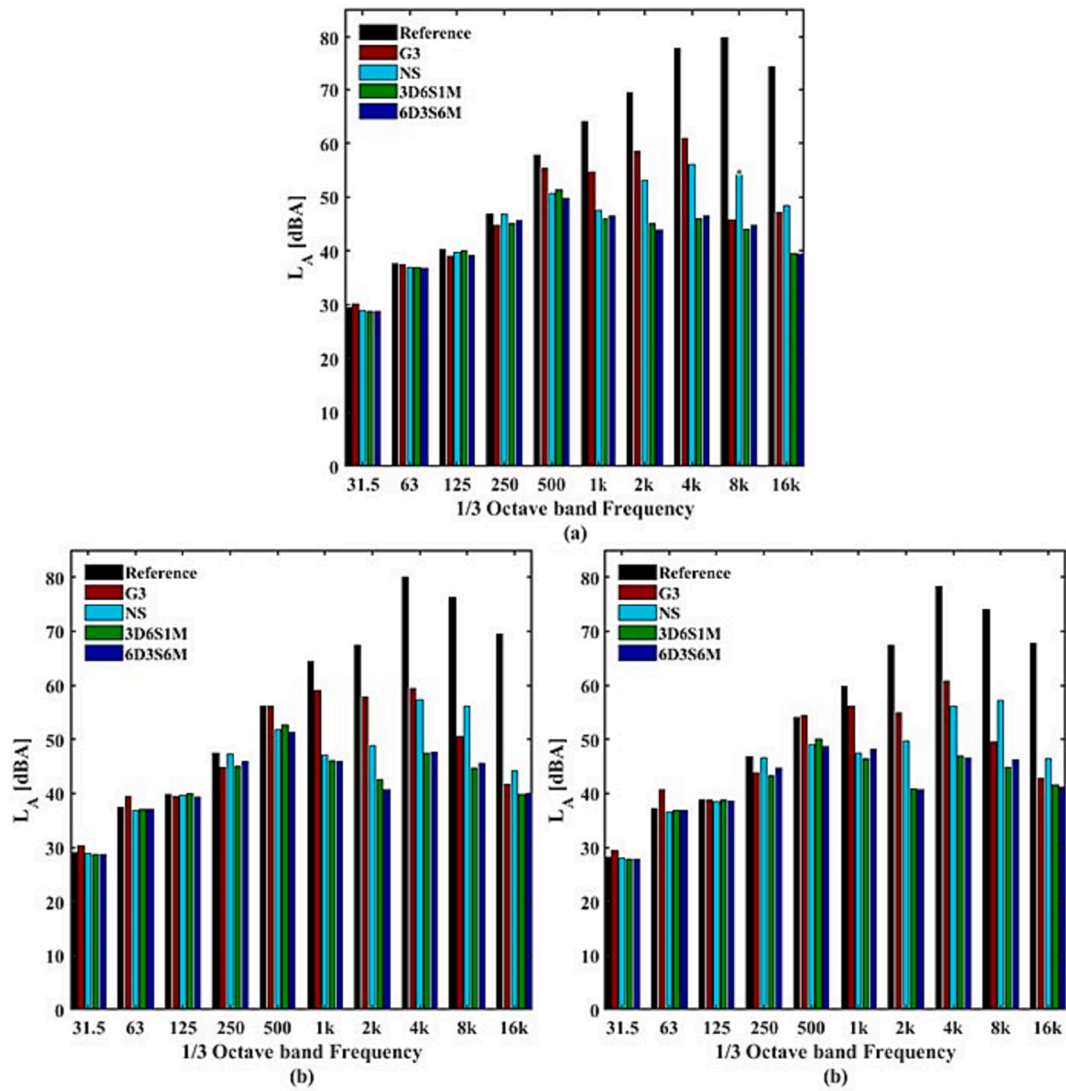


Fig. 10. A-weighted octave band SPL spectra of pneumatic silencers at (a) $\theta = 30^\circ$, (b) $\theta = 45^\circ$, and (c) $\theta = 60^\circ$.

Table 3
OASPL values of compressor exhaust noise.

Case	OASPL [dB]		
	30°	45°	60°
Reference	79.1	76.0	73.6
G3	53.4	52.4	52.0
NS	54.3	54.2	54.0
3D3S2M	48.0	47.8	48.0
3D3S6M	48.2	48.0	47.9
3D6S1M	45.5	45.4	45.7
3D6S3M	47.1	46.9	47.0
6D3S2M	46.6	46.4	46.5
6D3S6M	46.0	45.8	45.8
6D6S1M	47.7	47.8	47.6
6D6S3M	46.8	46.5	46.5

the best exhaust time among the cases related to the developed silencer, with a delay of 0.17 s and DR of 2.1%.

In the case of the developed silencer, the exhaust time was delayed compared with the general pneumatic silencer cases. The exhaust times of G3, the general pneumatic silencer with the best noise reduction effect, and 3D6S1M, the developed silencer, were 9.16 and 9.35 s, respectively. 3D6S1M exhibited a delay of approximately 2% compared

with G3. Moreover, the exhaust time can be reduced by considering the exhaust area listed in Table 2 and improving the slit structure.

3.3. Acoustic measurement of PAM exhaust flow

The exhaust noise of a general pneumatic system was measured through the exhaust of a compressor, and an experiment was conducted to measure the exhaust noise after installing a general pneumatic silencer case and the newly developed silencers that mimicked shark gill slits at the exhaust outlet of the PAM. The PAM exhaust noise measurement experiment was conducted for a duration of 4 s, starting from 1 s into the measurement.

First, the sound pressure generated during exhaust through the solenoid valve was measured by adjusting the initial pressure P_i of the PAM using a regulator, filling it successively to 8, 6, and 4 bar. Fig. 12 shows the sound pressure measurements of G3, 3D6S1M, and 6D3S2M for each initial pressure P_i at $\theta = 45^\circ$. In Fig. 12 (a), (d), and (g), as P_i increases, the sound pressure fluctuation decreases. However, in the silencer that mimicked shark gill slits, the peak noise caused by the solenoid valve decreased at 1 s; however, the subsequent sound pressure fluctuation tended to decrease slightly. Additionally, the results of the compressor exhaust experiment exhibited a trend similar to that of the general pneumatic silencer case in Fig. 6 (d), unlike the decrease in sound pressure after the peak noise in the G3 case. Excluding the peak

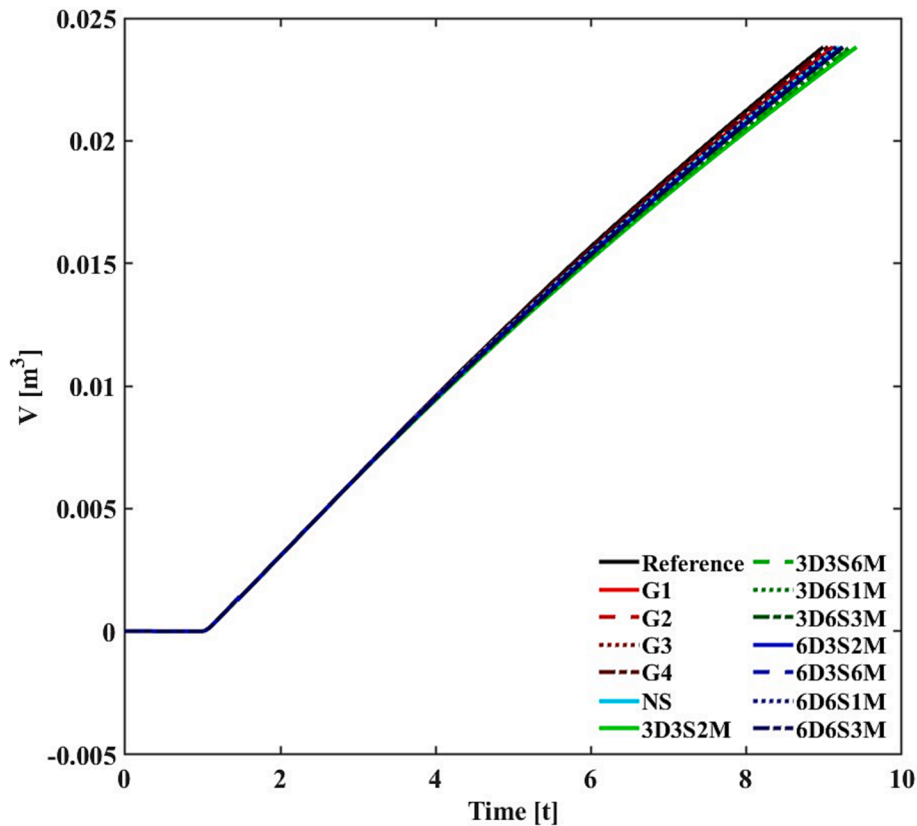


Fig. 11. Exhaust air volume of compressor exhaust noise for different pneumatic silencer configurations.

Table 4
Exhaust air volume and DR of compressor exhaust noise.

Case	Time at 0.024 m ³ [s]	DR [%]	Case	Time at 0.024 m ³ [s]	DR [%]
Reference	9	0	3D3S6M	9.37	4.6
G1	9.13	1.7	3D6S1M	9.35	4.3
G2	9.12	1.5	3D6S3M	9.27	3.3
G3	9.16	2.0	6D3S2M	9.25	3.2
G4	9.06	0.8	6D3S6M	9.25	3.1
NS	9.21	2.6	6D6S1M	9.17	2.1
3D3S2M	9.43	5.3	6D6S3M	9.25	3.2

noise at 1 s, the sound pressure at $P_i = 8$ bar in the shark gill slits mimicking noise-reducing device was lower than that in G3 at $P_i = 4$ bar.

Fig. 13 presents the OASPL for each case at P_i values of 8 bar and 6 bar, and Table 5 presents the corresponding OASPL values. Compared with the compressor exhaust noise measurement experiment, the results in Fig. 13 show that the OASPL of the 6D6S1M case was high, at approximately 47 dB, along with those of the G3 and NS cases. Moreover, the initial pressure of PAM, $P_i = 6$ bar, showed that the values of the 3D6S1M and 3D3S2M cases at $\theta = 45^\circ$ and $\theta = 60^\circ$ exhibited a more significant decrease than those at $\theta = 30^\circ$. When comparing the noise reduction effect of the developed silencer to that of the G3 case, the 3D6S1M case showed the best effect, with a reduction of approximately 5.7 dB at $P_i = 8$ bar and 5.7 dB at $P_i = 6$ bar when $\theta = 30^\circ$. In addition, the 6D3S2M case showed the best effect among the 6D cases, which differed from the compressor exhaust measurement experiment, where 6D3S6M had the best noise reduction effect. In comparison with the G3 case, the 6D3S2M case showed a noise reduction effect of 5.2 dB at $P_i = 8$ bar and 4.4 dB at $P_i = 6$ bar when $\theta = 30^\circ$.

Figs. 14 and 15 show the SPL spectrum of the G3, 3D6S1M, and 6D3S2M cases at $\theta = 60^\circ$ with A-weighted octave bands and SPL spectra,

respectively. Fig. 10 shows that the developed silencer had a low L_A at 1 kHz; however, in the exhaust noise measurement experiment of the PAM presented in Fig. 15, L_A of the developed silencer was higher than that of the reference at 1 kHz. Furthermore, the L_A of the developed silencer was higher than that of G3 at this frequency. Additionally, the NS case exhibited a tendency for the L_A to be higher than that of G3 above 8 kHz. In both (a) and (b) of the 6D3S2M case, the L_A at 16 kHz was higher than that of the 3D6S1M case. Furthermore, the L_A of the 3D6S1M case was the lowest above 4 kHz, thus demonstrating a good noise reduction effect.

4. Conclusion

The experimental results demonstrated that the developed silencer, which mimics shark gill slits, has superior noise reduction performance compared with the conventional pneumatic silencer in both compressor and PAM exhaust noise measurements. The use of polyurethane foam and slit structures that mimic shark gill slits disperse the flow and pressure of the compressed air exhaust, thus resulting in reduced exhaust noise by decreasing its relative velocity with the surrounding air. The findings were as follows:

- (1) The developed biomimetic silencer with shark-gill-like slit structures exhibited superior noise reduction performance compared with a general pneumatic silencer in both compressed air and PAM exhaust noise measurements. In the 3D6S1M case, the measurement experiments for the exhaust noise of the compressor and PAM exhibited a reduction in noise of 7.9 and 5.7 dB, respectively, compared with the general pneumatic silencer.
- (2) The slit structure inside the developed device, which mimicked shark gill slits, further reduced the exhaust noise. Despite the use of porous materials in the silencer, the exhaust time delay was

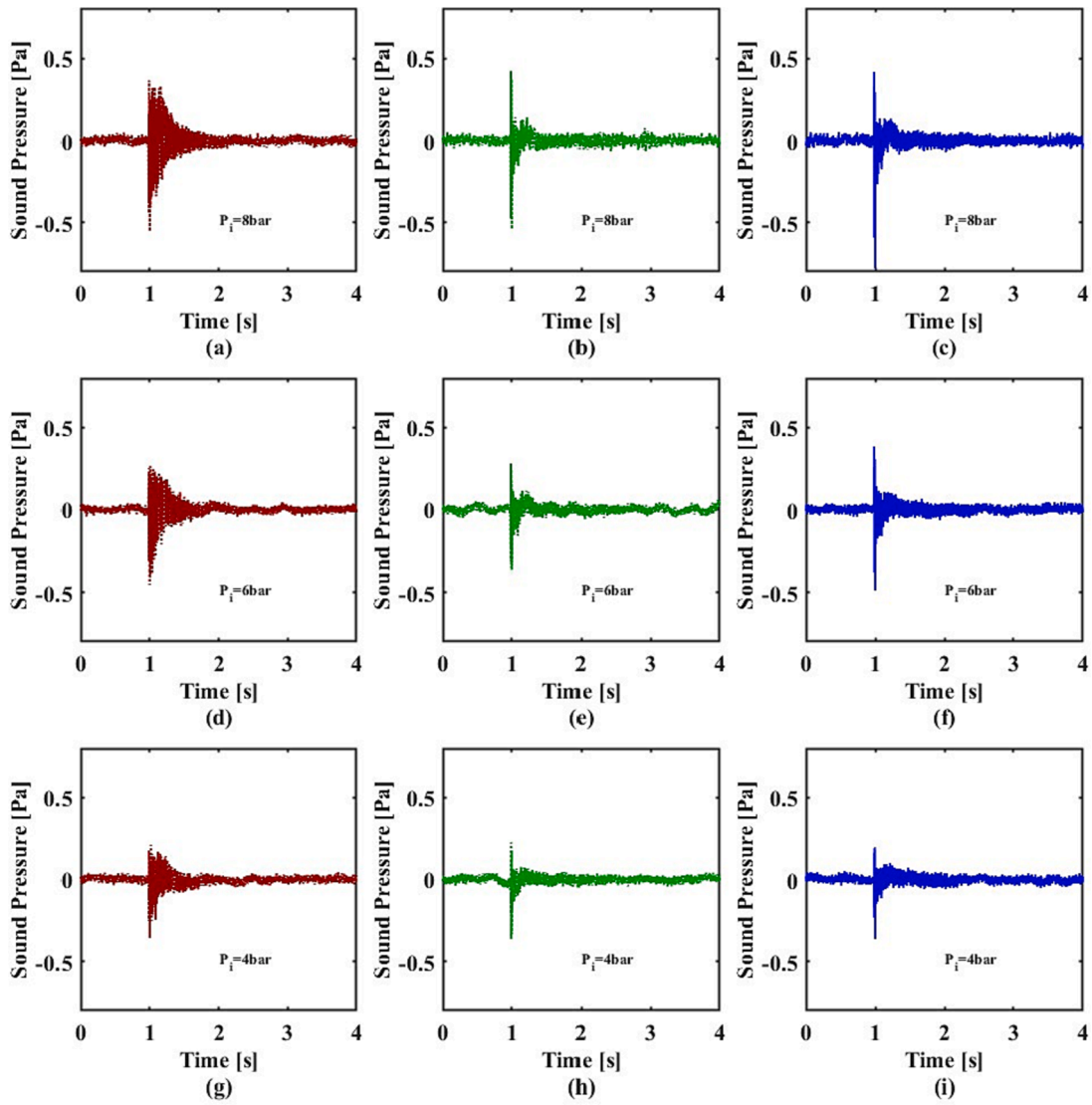


Fig. 12. Sound pressure of PAM exhaust noise measured at $\theta = 45^\circ$ under various initial pressure conditions: (a), (d), (g) G3 case at 8, 6, 4 bar; (b), (e), (h) 3D6S1M case at 8, 6, 4 bar; (c), (f), (i) 6D3S2M case at 8, 6, 4 bar.

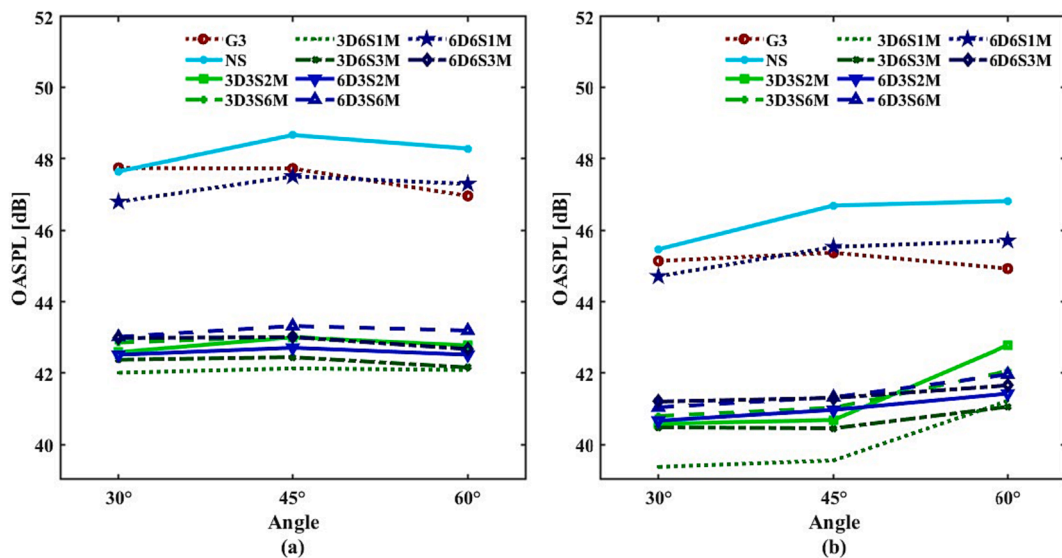


Fig. 13. OASPLs at angles of $\theta = 30^\circ, 45^\circ, 60^\circ$ for PAM initial pressures of 8 and 6 bar: (a) $P_i = 8\text{ bar}$ and (b) $P_i = 6\text{ bar}$.

Table 5
OASPL values of PAM exhaust noise.

Case	OASPL [dB] at $P_i = 8$ bar			OASPL [dB] at $P_i = 6$ bar		
	30°	45°	60°	30°	45°	60°
Reference	75.9	74.5	71.3	72.6	71.3	68.7
G3	47.7	47.7	47.0	45.1	45.4	44.9
NS	47.6	48.7	48.3	45.5	46.7	46.8
3D3S2M	42.6	43.0	42.8	40.6	40.7	42.8
3D3S6M	42.9	43.0	42.7	40.8	41.0	42.1
3D6S1M	42.0	42.1	42.1	39.4	39.6	41.2
3D6S3M	42.4	42.4	42.2	40.5	40.5	41.1
6D3S2M	42.5	42.7	42.5	40.7	41.0	41.4
6D3S6M	43.0	43.3	43.2	41.0	41.3	42.0
6D6S1M	46.8	47.5	47.3	44.7	45.5	45.7
6D6S3M	43.0	43.0	42.7	41.2	41.3	41.7

insignificant compared with that of a general pneumatic silencer in terms of the exhaust area, thus indicating its potential for application to pneumatic devices that require a fast response time, such as a PAM.

These findings suggest that the developed silencer is an effective solution for reducing exhaust noise in pneumatic devices, particularly in situations where noise reduction is critical. The use of the developed silencer is expected to help mitigate the problem of exhaust noise caused by the operation of pneumatic devices such as PAMs in daily life.

Although the experimental results demonstrated the superior noise reduction performance of the biomimetic silencer mimicking shark gill slits compared with a general pneumatic silencer, its application is limited. First, in the case of pneumatic devices such as a PAM, the exhaust is caused not only by the pressure difference but also by the volume change. Consequently, the different flow characteristics of the PAM and compressors may lead to changes in the flow pattern inside the silencer. Therefore, further research is necessary to optimize the slit structure that mimics shark gill slits and the porous material of the silencer to account for different flow characteristics. Secondly, the use of porous materials in the silencer causes an exhaust time delay, which may affect the performance of pneumatic devices requiring fast response times. To address these limitations, future studies can employ computational fluid dynamics analysis to analyze the flow characteristics inside the silencer owing to the slit structure and carry out further research

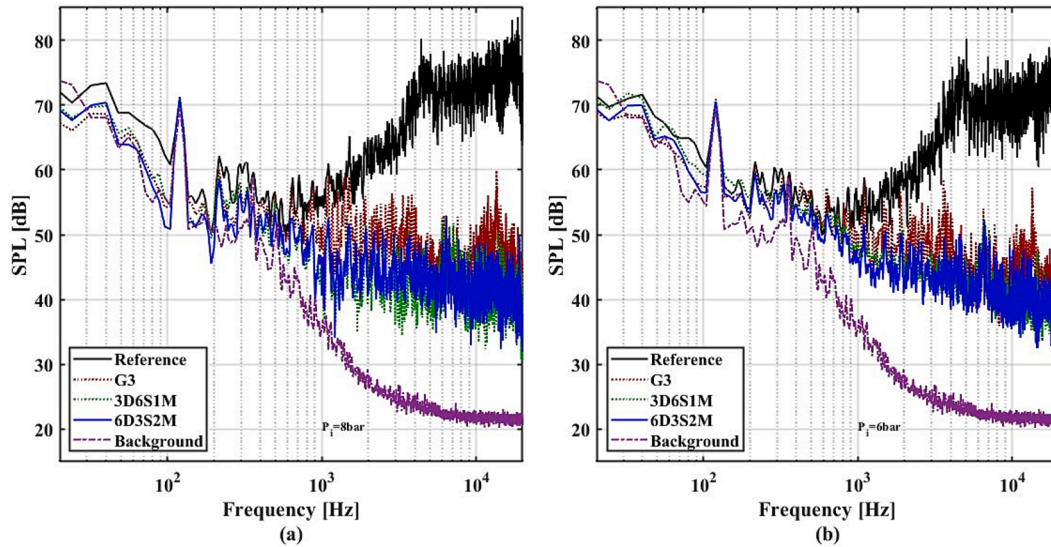


Fig. 14. Comparison of SPL spectra of pneumatic silencers at $\theta = 60^\circ$: (a) $P_i = 8$ bar and (b) $P_i = 6$ bar.

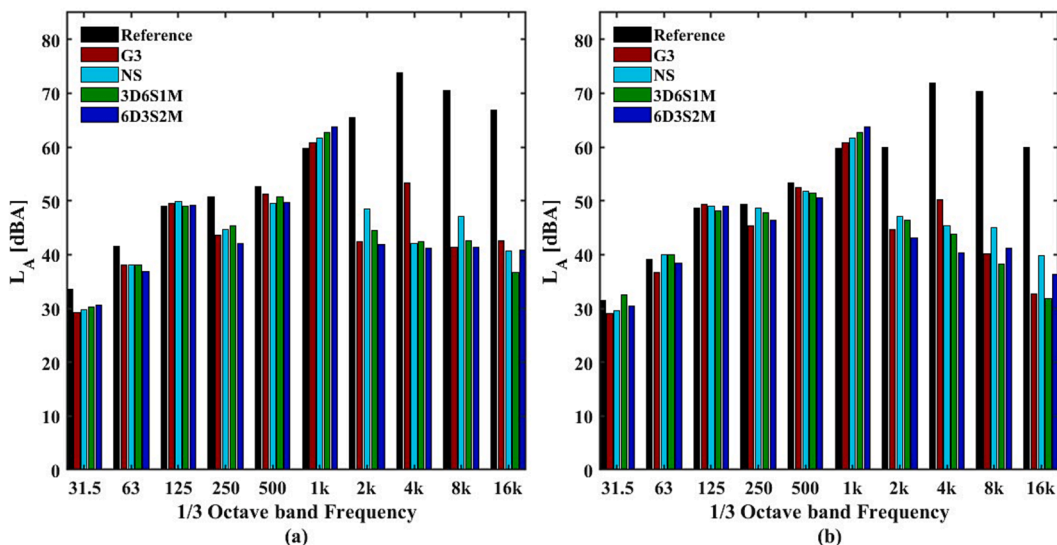


Fig. 15. A-weighted octave band SPL spectra of pneumatic silencers at $\theta = 60^\circ$: (a) $P_i = 8$ bar and (b) $P_i = 6$ bar.

to optimize both the structure and material based on these results.

CRedit authorship contribution statement

Min Hyeong Ahn: Conceptualization, Methodology, Investigation, Data curation, Writing – original draft. **Jihoon Kim:** Conceptualization, Investigation, Writing – review & editing. **Seung Ryeol Lee:** Conceptualization, Methodology, Writing – review & editing. **Ui Deok Lee:** Methodology, Investigation, Writing – review & editing. **Seunggi Kim:** Methodology, Investigation, Writing – review & editing. **Dongjun Shin:** Conceptualization, Methodology, Investigation, Writing – review & editing. **Hyungsoo Lee:** Formal analysis, Funding acquisition, Project administration, Supervision, Writing – review & editing. **Jaiyoung Ryu:** Formal analysis, Funding acquisition, Project administration, Supervision, Writing – review & editing.

Declaration of Competing Interest

The authors declare that they have no known competing financial interests or personal relationships that could have appeared to influence the work reported in this paper.

Data availability

Data will be made available on request.

Acknowledgments

This research was supported by the MIST (Ministry of Science and ICT), Korea, under the ITRC (Information Technology Research Center) support program (IITP-2020-2020-0-01655) supervised by the IITP (Institute of Information & Communications Technology Planning & Evaluation).; Industrial Technology Innovation Program [grant number 20007058, Development of safe and comfortable human augmentation hybrid robot suit] funded by the Ministry of Trade, Industry & Energy (MOTIE) of the Republic of Korea; and a Korea University Grant.

References

- [1] y Duran BM. Model-based control of a one-dimensional pendulum actuated with Pleated Pneumatic Artificial Muscles with adaptable stiffness: Master's thesis; 2005.
- [2] Muramatsu H, Ono H, Adachi M, editors. Development of a New Pneumatic Silencer to reduce unpleasantness of a sound. Proceedings of the JFPS International Symposium on Fluid Power. The Japan Fluid Power System Society; 2005.
- [3] Kim SJ, Chang H, Park J, Kim J. Design of a portable pneumatic power source with high output pressure for wearable robotic applications. *IEEE Robot Autom Let* 2018;3(4):4351–8.
- [4] Han K, Kim N-H, Shin D. A novel soft pneumatic artificial muscle with high-contraction ratio. *Soft Rob* 2018;5(5):554–66.
- [5] Ito T, Kogiso K, editors. Hybrid modeling of McKibben pneumatic artificial muscle systems. 2011 IEEE International Conference on Industrial Technology. IEEE; 2011.
- [6] Münzel T, Schmidt FP, Steven S, Herzog J, Daiber A, Sørensen M. Environmental noise and the cardiovascular system. *J Am Coll Cardiol* 2018;71(6):688–97.
- [7] Muzet A. Environmental noise, sleep and health. *Sleep Med Rev* 2007;11(2):135–42.
- [8] Ahmadabadi ZN, Laville F, Guilbault R. Time domain identification and ranking of noise sources in a pneumatic nail gun. *Appl Acoust* 2016;114:191–202.
- [9] Terashima FJH, de Lima KF, Barbieri N, Barbieri R, Legat Filho NLM. A two-dimensional finite element approach to evaluate the sound transmission loss in perforated silencers. *Appl Acoust* 2022;192:108694.
- [10] Leclere Q, Pezerat C, Laulagnet B, Polac L. Application of multi-channel spectral analysis to identify the source of a noise amplitude modulation in a diesel engine operating at idle. *Appl Acoust* 2005;66(7):779–98.
- [11] Zhang X, Yao Z, He F. Numerical simulation of the flow field of a diffused pneumatic silencer. *App Math Model* 2009;33(10):3896–905.
- [12] Li J, Zhao S, Ishihara K. Study on acoustical properties of sintered bronze porous material for transient exhaust noise of pneumatic system. *J Sound Vib* 2013;332(11):2721–34.
- [13] Li J, Zhao S. Optimization of valve opening process for the suppression of impulse exhaust noise. *J Sound Vib* 2017;389:24–40.
- [14] Laffay P, Moreau S, Jacob MC, Regnard J. Experimental study of the noise radiated by an air flow discharge through diaphragms and perforated plates. *J Sound Vib* 2018;434:144–65.
- [15] Gama NV, Ferreira A, Barros-Timmons A. Polyurethane foams: Past, present, and future. *Materials* 2018;11(10):1841.
- [16] Yuan B, Fang X, Liu J, Liu Y, Zhu R. Improved sound absorption properties in polyurethane foams by the inclusion of Al₂O₃ nanoparticles. *Shock Vib* 2021;2021:1–8.
- [17] Ye J, Xu M, Xing P, Cheng Y, Meng D, Tang Y, et al. Investigation of aerodynamic noise reduction of exterior side view mirror based on bionic shark fin structure. *Appl Acoust* 2021;182:108188.
- [18] Kim DH, Cheol SY, Iyer RS, Kim HD. A newly designed entrance hood to reduce the micro pressure wave emitted from the exit of high-speed railway tunnel. *Tunn Undergr Sp Tech* 2021;108:103728.
- [19] Gad-el-Hak I, Mureithi N. Mitigation of jet cross-flow induced vibrations using an innovative biomimetic nozzle design inspired by shark gill geometry. *Sci Rep* 2022;12(1):11107.
- [20] Muir B, Kendall J. Structural modifications in the gills of tunas and some other oceanic fishes. *Copeia* 1968;388–98.
- [21] Lighthill MJ. Jet noise. *AIAA J* 1963;1(7):1507–17.
- [22] Lighthill MJ. On sound generated aerodynamically I. General theory. *Proc Roy Soc London Series A Math Phys Sci* 1952; 211(1107): 564–87.
- [23] Lighthill MJ. On sound generated aerodynamically II. Turbulence as a source of sound. *Proc Roy Soc London Series A Math Phys Sci* 1954; 222(1148): 1–32.
- [24] Zou G, She J, Peng S, Yin Q, Liu H, Che Y. Two-dimensional SEM image-based analysis of coal porosity and its pore structure. *Int J Coal Sci Technol* 2020;7:350–61.
- [25] Xavier MS, Fleming AJ, Yong YK. Design and control of pneumatic systems for soft robotics: A simulation approach. *Ieee Robot Autom Let* 2021;6(3):5800–7.
- [26] Lush P. Measurements of subsonic jet noise and comparison with theory. *J Fluid Mech* 1971;46(3):477–500.
- [27] Oppenheim AV. Discrete-time signal processing. Pearson Education India; 1999.